Crystal Structure of GDP-Mannose Dehydrogenase: A Key Enzyme of Alginate Biosynthesis in *P. aeruginosa*[†,‡]

Christopher F. Snook, Peter A. Tipton, and Lesa J. Beamer*

Department of Biochemistry, 117 Schweitzer Hall, University of Missouri−Columbia, Columbia, Missouri 65211

Received December 9, 2002; Revised Manuscript Received February 13, 2003

ABSTRACT: The enzyme GMD from *Pseudomonas aeruginosa* catalyzes the committed step in the synthesis of the exopolysaccharide alginate. Alginate is a major component of *P. aeruginosa* biofilms that protect the bacteria from the host immune response and antibiotic therapy. The 1.55 Å crystal structure of GMD in ternary complex with its cofactor NAD(H) and product GDP-mannuronic acid reveals that the enzyme forms a domain-swapped dimer with two polypeptide chains contributing to each active site. The extensive dimer interface provides multiple opportunities for intersubunit communication. Comparison of the GMD structure with that of UDP-glucose dehydrogenase reveals the structural basis of sugar binding specificity that distinguishes these two related enzyme families. The high-resolution structure of GMD provides detailed information on the active site of the enzyme and a template for structure-based inhibitor design.

Pseudomonas aeruginosa is an opportunistic human pathogen that causes life-threatening infections in CF,[1] burn, and immuno-compromised patients. Lung infections by *P. aeruginosa* can begin early in the life of CF patients, and despite aggressive antibiotic therapy, often lead to irreversible lung damage and respiratory failure (*1*). In the CF lung, *P. aeruginosa* frequently undergoes a phenotypic conversion to a mucoid state that is associated with the chronic phase of infection and correlated with a poor patient prognosis. Mucoid strains of *P. aeruginos*a secrete large quantities of the viscous exopolysaccharide alginate. The production of alginate is believed to afford protection from the host immune response and antibiotic therapy and promotes persistence of the bacteria in the respiratory tract (*2*). Alginate is important for the development of mature *P. aeruginosa* biofilms and dramatically increases their resistance to antimicrobial treatments (*3*).

A potential strategy for combating *P. aeruginosa* infection is to block alginate biosynthesis through application of specific inhibitors of the biosynthetic enzymes. A logical target for inhibition is GDP-mannose dehydrogenase (GMD), a key regulatory enzyme in the alginate biosynthetic pathway of *P. aeruginosa*. GMD catalyzes the committed step of the alginate biosynthetic pathway, and metabolic studies have shown that GMD is a rate-limiting enzyme in mucoid strains of *P. aeruginosa* (*4*). Inhibitors of GMD have been shown to increase the sensitivity of a mucoid strain of *P. aeruginosa* to tobramycin, a commonly used antibiotic for CF lung infections (*5*). Thus, effective inhibitors of GMD could be expected to block alginate production and interfere with normal biofilm formation in chronic *P. aeruginosa* infections and may be useful adjuvants to conventional antibiotic treatment. Since there is no corresponding enzyme in humans, specific inhibition of its activity should produce few deleterious side effects.

GMD is the product of the *algD* gene and catalyzes the essentially irreversible conversion of GDP-mannose to GDP-mannuronic acid. This nucleotide sugar is used by the bacterium solely for alginate synthesis, where it acts as the donor to a precursor homopolymer of β-mannuronic acid. After secretion into the periplasm, the homopolymer is modified by epimerization and acetylation to produce mature alginate, a (1 → 4) linked linear copolymer of β-D-mannuronic acid and its C-5 epimer α-L-guluronic acid (*6*). Although several of the genes involved in alginate biosynthesis have recently been shown to have multiple homologues in the *P. aeruginosa* genome, none have been identified for *algD* (*7*).

GMD is a member of a small group of NAD^+-dependent four-electron-transfer dehydrogenases, which includes UGD, histidinol dehydrogenase, and 3-hydroxy-3-methylglutaryl-CoA reductase. The latter two proteins are structurally and mechanistically distinct from GMD (*8*, *9*). However, UGD and GMD are believed to be mechanistically similar, utilizing a single active site to catalyze the two-step conversion of an alcohol to the corresponding acid via a thiohemiacetal intermediate (Figure 1A). The crystal structure of UGD from *Streptococcus pyogenes* has been reported (*10*) and shows that the enzyme exists as a dimer. *P. aeruginosa* GMD (*11*) shows both allosteric and cooperative behavior, implying a higher order oligomeric state consistent with previous biochemical characterization of the enzyme (*12*). Here, we report determination of the crystal structure of *P. aeruginosa*

[†] Supported by NIH Grant GM59653. Use of the Advanced Photon Source was supported by the U.S. Department of Energy Basic Energy Sciences, Office of Science, under Contract W-31-109-Eng-38.

[‡] The coordinates of the 1.55, 2.0, and 2.8 Å GMD structures have been deposited with the Protein Data Bank and assigned the codes 1MV8, 1MUU, and 1MF2, respectively.

* Corresponding author. Tel: (573) 882-6072. Fax: (573) 884-4812. E-mail: beamerl@missouri.edu.

[1] Abbreviations: GMD, GDP-mannose dehydrogenase; CF, cystic fibrosis; UGD, UDP-glucose dehydrogenase; SeMet, selenomethionine; PEG, poly(ethylene glycol); MAD, multiwavelength anomalous diffraction; rmsd, root-mean-square-deviation.

10.1021/bi027328k CCC: $25.00
Published on Web 04/02/2003

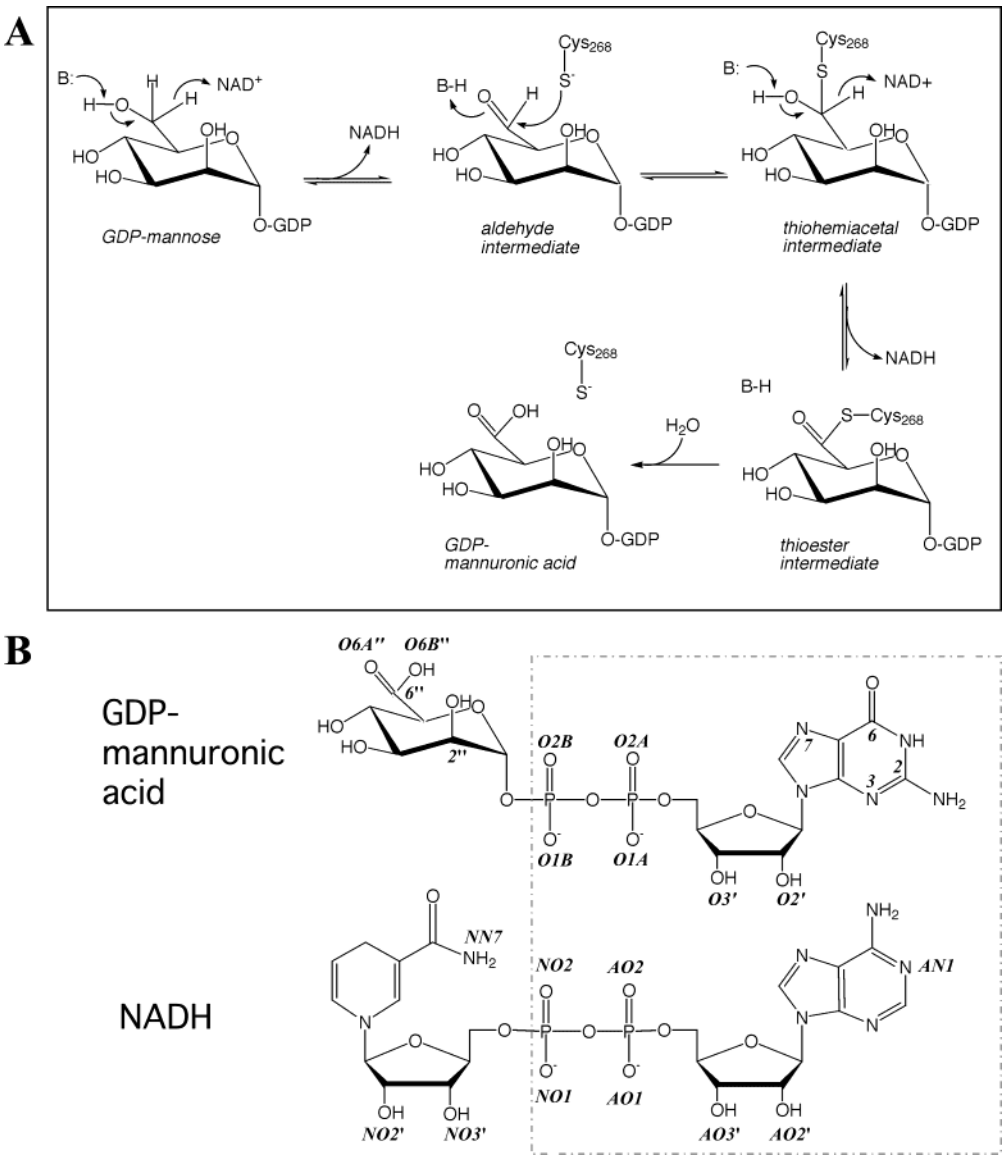

FIGURE 1: (A) Proposed mechanism for GDP-mannose dehydrogenase. The reaction is a two-step conversion of GDP-mannose to GDP-mannuronic acid utilizing 2 equiv of NAD^+. Initial oxidation of the substrate C6″ hydroxyl group to an aldehyde is followed by addition of the Cys268 side chain to form a thiohemiacetal, a second oxidation to produce the thioester intermediate, and hydrolysis to form the product. (B) A comparison of the structures of the NADH and GDP-mannuronic acid. Similar structural features of the two ligands are highlighted in the dashed box. Atom names for the two ligands are shown in italicized bold type.

GMD in complex with its cofactor NAD(H) and reaction product, GDP-mannuronic acid (Figure 1B). In combination with ongoing mechanistic studies, this structure provides a detailed template for future efforts at inhibitor design.

MATERIALS AND METHODS

Crystallization and Data Collection. Wild-type and SeMet-substituted GMD proteins were purified as previously described (*11*). The SeMet protein was produced in *Escherichia coli* by growing bacteria in minimal media and in the presence of SeMet, lysine, threonine, phenylalanine, leucine, isoleucine, and valine to inhibit methionine biosynthesis (*13*). Incorporation of nine SeMet residues was verified by MALDI mass spectrometric analysis (Mass Consortium, La Jolla, CA; data not shown). After determination of the structure, it was found that both the wild-type and the SeMet proteins cocrystallized with NAD(H) and GDP-mannuronic acid, which apparently co-purified with the enzyme.

Both wild-type and SeMet proteins were dialyzed into 50 mM HEPES pH 7.5, 1.0 mM dithiothreitol and crystallized by hanging drop vapor diffusion using a 1:1 ratio of protein to well buffer and a protein concentration of approximately 7.5 mg/mL. Native GMD crystallized in 8% methylpentanediol and 0.1 M Na acetate buffer at pH 4.6 in space group $P4_3$. The SeMet protein crystallized isomorphously with the native crystals but under different conditions. The most reproducible SeMet crystals were grown from 2% PEG 3350, 20 mM magnesium sulfate, and 0.1 M Na acetate buffer at pH 4.8. Both the native and the SeMet GMD crystals in space group $P4_3$ exhibited variable and unpredictable degrees of merohedral twinning, ranging from 5 to 45%. Attempts to eliminate or reduce twinning by varying crystallization conditions were unsuccessful. A different form of the SeMet crystals grew irreproducibly in space group $C222_1$ from 10% PEG 3350, 20% 2-propanol, and 0.1 M Na citrate buffer at pH 5.6. Cryoprotection of crystals was performed by either

Table 1: Crystallographic and Data Collection Statistics

crystal	SeMet			native	SeMet
space group	$P4_3$			$P4_3$	$C222_1$
unit cell parameters (Å)	$a = b = 82.5$ $c = 310.2$			$a = b = 82.4$ $c = 309.9$	$a = 131.2$ $b = 136.8$ $c = 218.6$
twinning fraction (%)	24.5			17.4	
# chains/asymmetric unit	4			4	4
mosaicity (deg)	0.23			0.21	0.53
	MAD data				
	λ 1	λ 2	λ 3		
wavelength (Å)	0.97934	0.97947	0.94225	0.97934	1.54
resolution (Å)	1.90	1.90	2.05	1.55	2.8
R_{sym}[a] (%)	9.4 (33.6)[b]	8.6 (41.8)	8.8(33.8)	12.3 (39.1)	6.5 (21.7)
R_{anom}[c] (%)	5.8	4.4	5.1		
unique reflections	158 133	158 540	129 450	294 277	48 049
observed reflections	1 087 877	1 096 050	975 001	1 557 003	151 736
completeness (%)	97.8 (90.7)	97.8 (90.7)	99.7 (99.4)	99.0 (97.0)	98.7 (90.0)
$I/\sigma(I)$	28.0 (3.3)	30.1 (3.1)	15.4 (4.0)	20.3 (2.1)	16.7 (4.4)

[a] $R_{sym} = \sum|I_h - \langle I_h \rangle| / \sum|I_h|$ where $\langle I_h \rangle$ is the average intensity over symmetry equivalents. [b] Numbers in parentheses refer to statistics for the highest resolution shell. [c] $R_{anom} = \sum||F_{PH}^+| - |F_{PH}^-|| / \sum(|F_{PH}^+| - |F_{PH}^-|)/2$.

quick dips or prolonged soaks into a solution of 50% saturated sucrose in the respective crystallization buffers.

A three wavelength MAD data set and a high-resolution native data set on the $P4_3$ crystals were collected at −180 °C at beam line SBC 19-ID at the Advanced Photon Source of Argonne National Laboratory. A data set for the $C222_1$ crystal form was collected in-house on a Rigaku RU200 rotating anode at −160 °C. Data were indexed and integrated with the HKL package (*14*). Statistics for the X-ray diffraction data are presented in Table 1.

Structure Solution and Refinement. Despite significant twinning of the GMD diffraction data (Table 1), 30 of the 36 possible SeMet sites in the asymmetric unit of the $P4_3$ crystals were located and refined using the program SOLVE (*15*). Final Z-score and figure of merit to 2.0 Å were 31.5 and 0.43, respectively. Density modification of phases from SOLVE was done with RESOLVE (*16*) yielding high quality electron density maps (figure of merit = 0.58). The initial model was built using the automatic chain-tracing feature of RESOLVE that placed approximately 1450 of the 1744 residues in the tetramer. The model was completed interactively using O (*17*) and refined with REFMAC 5.0 (*18*) with individual, restrained B-factors. Progress was monitored by use of R_{free}, and 5% of the data were set aside for cross-validation before refinement. Water molecules were placed automatically by WATPEAK (*18*) in peaks greater than 3.0 σ in $F_o - F_c$ maps and within hydrogen bonding distance to nitrogen or oxygen atoms of the protein. No noncrystallographic symmetry restraints were used at any point during refinement of this or other data sets. The Matthew's coefficient for these crystals is 2.76 (Å^3 Da^{-1}) and corresponds to 55% solvent content. No clear electron density was present for the nicotinamide ring of NAD(H) so this portion of the cofactor has been omitted from the model. One round of TLS refinement (*19*) was done on the final model, using the four protein chains in the asymmetric unit as rigid bodies. Density for the side chains of 134 of the 1744 residues in the asymmetric unit was not well-defined, and they were truncated to alanine. Refinement statistics are shown in Table 2.

Table 2: Refinement Summary

	SeMet $P4_3$	native $P4_3$	SeMet $C222_1$
resolution range (Å)	40.0−2.0	40.0−1.55	40.0−2.8
R_{cryst}[a]	20.9	17.4	20.7
R_{free}[b]	23.4	19.4	26.3
rmsd bond distance (Å)	0.012	0.010	0.014
rmsd bond angle (deg)	1.4	1.4	1.3
total no. non-H atoms in asu	14 082	14 878	13 281
no. of solvent molecules	903	1375	106
avg. protein B-value (Å^2)	19.7	9.4	34.7
avg. solvent B-value (Å^2)	36.1	31.0	26.8
heteroatoms	4 NAD(H)[c] 4 GMA 1 sucrose	4 NAD(H)[c] 4 GMA 2 sucrose	4 GMA

[a] $R_{cryst} = \sum|F_o - F_c| / \sum|F_c|$ where F_o and F_c are observed and calculated structure factors, respectively. [b] R_{free} is the R factor calculated from 5% of the reflections not included in refinement. GMA = GDP − mannuronic acid. No σ-cutoff of the data was used. [c] The NAD(H) cofactor in the deposited models does not include the nicotinamide ring.

The 2.0 Å model of the SeMet protein was used for rigid-body refinement against the 1.55 Å native GMD data. The model was further refined with REFMAC 5.0 (*18*) with individual, restrained B-factors. After several cycles of refinement and manual rebuilding, R_{cryst} and R_{free} converged at 19.9 and 21.9%, somewhat high for 1.55 Å resolution data. To see if this was due to twinning of the data, the reflection file was detwinned with DETWIN (*20*) (maintaining the same test set), and the model was subjected to further rounds of refinement. This improved the R_{cryst} and R_{free} to 17.9 and 19.8%. TLS refinement was done as above. Waters and NAD(H) were built as above. Density for the side chains of 50 of the 1744 residues in the asymmetric unit was not well-defined, and they were truncated to alanine. Refinement statistics are shown in Table 2.

Molecular replacement was performed with the $C222_1$ data set of SeMet GMD using the GMD dimer from the $P4_3$ crystal form as a search model. The program EPMR (*21*), which utilizes an evolutionary search algorithm, located two independent domain-swapped dimers of GMD in the asymmetric unit, giving a final correlation coefficient of 70.2% and a R-factor of 35.0%. In this space group, two GMD

dimers are related by a crystallographic 2-fold axis to produce the GMD tetramer observed in the $P4_3$ crystal form. The model was partially refined with REFMAC 5.0 (*18*), initially with an overall B-factor and later using individual, restrained B-factors. The final model of SeMet GMD in this space group contains four chains of 436 residues in the asymmetric unit, 110 water molecules, and four molecules of GDP-mannuronic acid. Since density for most of the NAD(H) was poorly ordered in all four active sites, the cofactor was not included in the model. Refinement statistics are shown in Table 2.

Model Quality. The 2.0 and 1.55 Å models have more than 90% of residues in the most favored region of the Ramachandran plot and are very similar (overall C_α rmsd of 0.2 A^2 for four molecules in the asymmetric unit). All models were examined with Procheck (*22*), Whatcheck (*23*), SFCHECK (*24*), and ERRAT (*25*). The size of the active site pocket was calculated with CAST (*26*), surface areas with the protein−protein interaction server (*27*), and superpositions with TOP (*28*). Figures 2−4 were prepared with MOLSCRIPT (*29*).

Modeling of Nicotinamide Ring. Because of poor density for the nicotinamide ring of NAD(H) in the 1.55 Å GMD structure, it was modeled by superimposing NAD(H) from the UGD structure on the corresponding incomplete molecule in the GMD model. This places the nicotinamide ring in a syn conformation and in a relatively open area of the active site, in close proximity to Cys268 and the carboxylate of the mannuronic acid, as would be required for catalysis. In its modeled position, some close steric contacts occur between the nicotinamide ring and the side chain of Glu157, several water molecules, and the carboxylate group of mannuronic acid. However, this arrangement is clearly preferable to the anti orientation that would clash with the backbone of the polypeptide chain.

RESULTS AND DISCUSSION

Overall Structure. The structure of *P. aeruginosa* GMD was determined by MAD phasing at 2.0 Å using crystals of selenomethionine-substituted protein and further refined to 1.55 Å with an isomorphous native data set (Tables 1 and 2). Features of the 1.55 Å model are described in the following sections. Enzyme−ligand hydrogen bonds (Table 3), including those mediated by water, represent interactions observed in all four active sites in the asymmetric unit. Throughout this manuscript, we refer to the bound cofactor as NAD(H) since the nicotinamide ring is not well-defined in electron density maps, and we are unable to distinguish between NAD^+ and NADH.

The crystal structure shows that GMD contains two distinct domains of similar size that are connected by a long (33-residue) α-helix (Figure 2A). Both the N- and the C-terminal domains have α/β topology with a central, twisted β-sheet flanked on each side by α-helices, typical of a dinucleotide-binding Rossmann fold (Figure 2B). The N-terminal domain (residues 1−202) contains a complete dinucleotide-binding motif, consisting of a 6-stranded parallel β-sheet and five α-helices. This is followed by an antiparallel β−α−β extension of the central β-sheet. The C-terminal domain (residues 235−436) begins with a cluster of three α-helices, which are followed by an incomplete dinucleotide-binding motif that is missing the third β-strand and final α-helix. Except for a few α-helical insertions in loop regions and the missing elements of the Rossmann fold, the two dinucleotide-binding motifs (residues 1−154 and 315−436) are quite similar to each other, with a rmsd of 1.1 $Å^2$ over 60 residues (Figure 2C). The sequence identity between the two domains, however, is only 22% and not detectable by standard homology searches such as BLAST (*30*), suggesting an ancient gene duplication of the dinucleotide-binding motif. The internal pseudo-2-fold symmetry of the GMD monomer has been observed in a number of other dehydrogenase structures (*31*).

The GMD monomer has an unusual open conformation with its N- and C-terminal domains on opposite sides of the connecting α-helix. Two of these open monomers associate to form a highly intertwined dimer that places the N-terminal domain of monomer A in close association with the C-terminal domain of monomer B (Figure 2D). By comparison with the structure of the related enzyme UGD, where the N- and C-terminal domains of the same chain pack against each other in a normal closed monomer, the GMD dimer can be described as domain-swapped. 3-D domain swapping has been proposed as a mechanism for creating oligomers from monomeric proteins, endowing them with evolutionary advantages such as cooperativity (*32*). Although it is possible that the domain swapping seen in the GMD structure is an artifact of protein purification or crystallization, we consider this unlikely since the protein retained cofactor and product during purification and because the swapping is seen in multiple crystal forms (see Materials and Methods).

Kinetic data have suggested that GMD forms an oligomer of at least six subunits in solution (*11*). The crystal form of GMD used to solve the structure (space group $P4_3$) contains four molecules in the asymmetric unit, raising the possibility of a tetrameric form of the protein. The putative tetramer interface has a total of 14 hydrogen bond pairs and buries approximately 1000 $Å^2$ of surface area per dimer. However, this accounts for only 3% of the total surface area of the dimer, and the surfaces involved in the interface are not particularly complementary (Figure 2E). To try to distinguish the tetramer interface from crystal lattice contacts, we used molecular replacement to solve the structure of an alternative crystal form of GMD (space group $C222_1$), which crystallized from a different precipitant and at a pH above the pI of the protein rather than below as in the $P4_3$ form. Despite these differences, the unit cell of the $C222_1$ crystals contains an essentially identical tetramer, supporting the possibility of a biologically relevant, although possibly rather weak, tetramer interface. Such an interface may be conducive to equilibrium between dimeric and tetrameric forms of the enzyme. Kinetic and light scattering data indicate varying oligomeric states of GMD under different conditions (*11*), and limited proteolysis experiments show that residues within the tetramer interface are protected from proteolysis in the presence of substrate (*33*). It is currently unclear how to reconcile the tetramer in the crystal with kinetic data indicating Hill coefficients for GMD of up to six (*11*).

Cofactor and Substrate/Product Binding Sites. On the basis of amino acid sequence comparisons and the structure of the related UGD protein, it was expected that the active site of GMD would lie in a cleft between its two domains, with the N-terminal domain being primarily responsible for

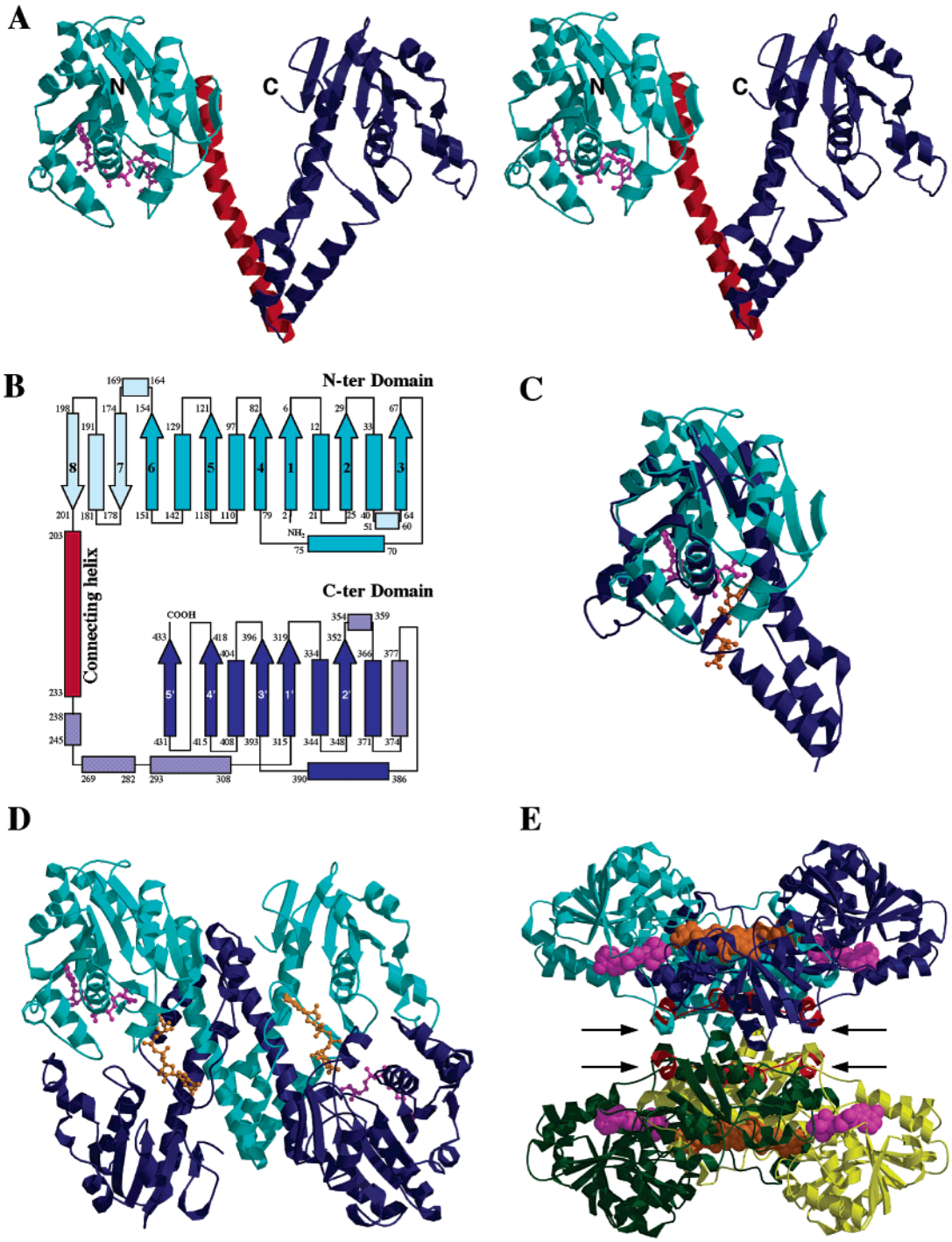

FIGURE 2: Structure and topology of GMD. (A) A stereoview ribbon diagram of the GMD monomer (residues 1−436) showing the N-terminal domain in cyan, the C-terminal domain in blue, and the connecting α-helix in red. The amino and carboxy termini are labeled N and C, respectively. NAD(H) and GDP-mannuronic acid are shown as ball-and-stick models in magenta and gold, respectively. (B) Topology diagram of the GMD monomer showing α-helices as rectangles and *β*-strands as arrows. Colors as in panel A. Structures that are not part of the classical dinucleotide-binding fold are in lighter shades. (C) Superposition of the N- and C-terminal domains of GMD with bound ligands, colors as in panel A. (D) The domain-swapped GMD dimer with monomer A shown in cyan and monomer B in blue. (E) The GMD tetramer with monomers A−D in cyan, blue, yellow, and green, respectively. NAD(H) and GDP-mannuronic acid are shown as space-filling models, colors as in panel A. Two positions (residues 275 and 298) are protected from proteolysis upon substrate binding; the loops between these residues are shown in red and highlighted with arrows (*33*).

binding the NAD(H) cofactor, while the connecting α-helix and C-terminal domain would make most of the contacts with the substrate/product. Electron density maps showing bound NAD(H) and GDP-mannuronic acid in all four active sites in the tetramer essentially confirm this expectation. However, because of the domain swapping, the two active sites in the dimer are hybrids, composed of residues from the N-terminal domain and connecting α-helix of monomer A and the C-terminal domain of monomer B. In total, more than 80 residues (approximately half from each monomer) come together in the active site to form a large binding pocket for NAD(H) and GDP-mannuronic acid, with a total surface area of approximately 1900 Å^2 (*26*). Both ligands are deeply buried (more than 90% of their total surface areas) in their

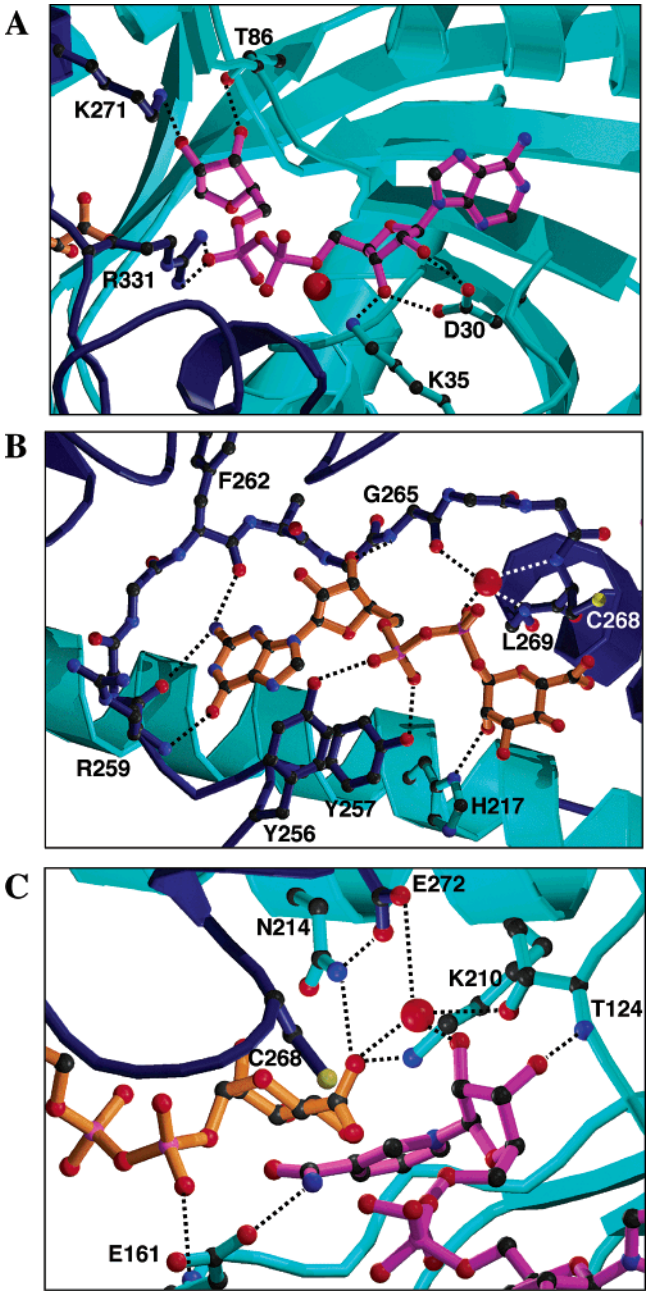

FIGURE 3: Close-up view of the ligand binding sites in GMD, emphasizing contacts made by two polypeptide chains. Monomer A is shown in cyan and monomer B in blue. (A) Binding pocket of NAD(H) (magenta) with selected contacting residues shown in ball-and-stick model. (B) GDP-mannuronic acid (gold) binding pocket highlighting multiple contacts by residues in a 15-residue stretch of monomer B. Also shown is a conserved water molecule that contacts the pyrophosphate group, and the contact made by His217. (C) Network of direct and water-mediated hydrogen bonds linking NAD(H) and GDP-mannuronic acid in the active site. The nicotinamide ring of NAD(H) is included in its modeled position.

binding sites, with only the edge of their purine bases exposed to solvent.

The binding site for the NAD(H) cofactor is formed primarily by amino acids in the N-terminal dinucleotide-binding motif of monomer A (Table 3 and Figure 3A). NAD(H) adopts an extended conformation similar to that seen in many NAD(H)-protein complexes and lies in a cleft near the carboxy ends of β-strands 1 and 4. Eight highly conserved protein residues make one or more direct hydrogen bonds with the cofactor. These include several conserved interactions typical of NAD-binding proteins, such as Tyr10 and Val11 in the phosphate-binding loop that donate hydrogen bonds from their main chain amides to the pyrophosphate group of NAD(H). The side chain of Asp30, another conserved residue in the Rossmann fold, forms hydrogen bonds with the two hydroxyls of the adenine ribose ring. Two residues from the C-terminal domain of monomer B contact the cofactor, Lys271 and Arg331, and form hydrogen bonds to the nicotinamide ribose ring and pyrophosphate group, respectively. When Lys271 is changed to glutamine, GMD loses activity (*6*). In addition to direct protein−NAD(H) contacts, several residues are involved in water-mediated hydrogen bonds, including one frequently observed water (*34*) that mediates contacts between the main chain amides of glycines 9 and 12 and the pyrophosphate group of the cofactor. In contrast to the multiple contacts with the pyrophosphate moiety and ribose sugars, only one water-mediated hydrogen bond to the adenine is observed, although several conserved hydrophobic residues (valines 31, 84, 102, and Tyr98) are in van der Waals contact with the base.

Unlike the rest of the NAD molecule, the nicotinamide ring is not well-defined in the electron density maps. This has been observed in other NAD(H)−protein complexes (*35*) and may be due to multiple rotational conformers of the ring or possibly hydrolysis of the glycosidic bond. For purposes of analysis, we have modeled a reasonable position for the nicotinamide ring (see Materials and Methods) and find that it makes one specific contact with the protein: a hydrogen bond between its carboxamide nitrogen and the side chain of Glu161, which may be important for anchoring it in the syn conformation. On the basis of this modeled position, we predict that the hydride is transferred to the si face of NAD^+, although the stereospecificity of this transfer has not yet been determined experimentally for GMD.

Despite the pseudosymmetry of the GMD monomer and structural similarity of the ligands (Figure 1B), the C-terminal domain of GMD binds its ligand in a very different orientation than the N-terminal domain and does not utilize its nucleotide-binding fold in a typical fashion (Figure 2B). The majority of protein contacts to GDP-mannuronic acid are made by residues in the 3-helix cluster of the C-terminal domain of monomer B (Table 3). The GDP-mannuronic acid adopts an extended conformation in its binding pocket, spanning more than 17 Å from N2 of the guanine to the carboxylate group of the mannuronic acid. One 15-residue stretch of the polypeptide chain (residues 257−272) makes an extensive series of contacts with the sugar nucleotide (Figure 3B), starting at the pyrophosphate group, looping around the guanine, and running lengthwise down the other edge of the molecule. This includes contacts from several residues in the active site signature sequence GGxCxxxD (residues 265−272) that is characteristic of the nucleotide−sugar dehydrogenases (*10*). The backbone amide of Gly265, for instance, hydrogen bonds to the O3′ hydroxyl of the ribose. Three residues within the signature sequence, Gly265, Cys268, and Leu269, also coordinate to make a contact via the same water molecule to the pyrophosphate group of the product. In contrast with the paucity of specific protein contacts to the adenine of NAD(H), a number of direct and water-mediated hydrogen bonds are made to the guanine by residues in the 3-helix cluster. These residues form a highly

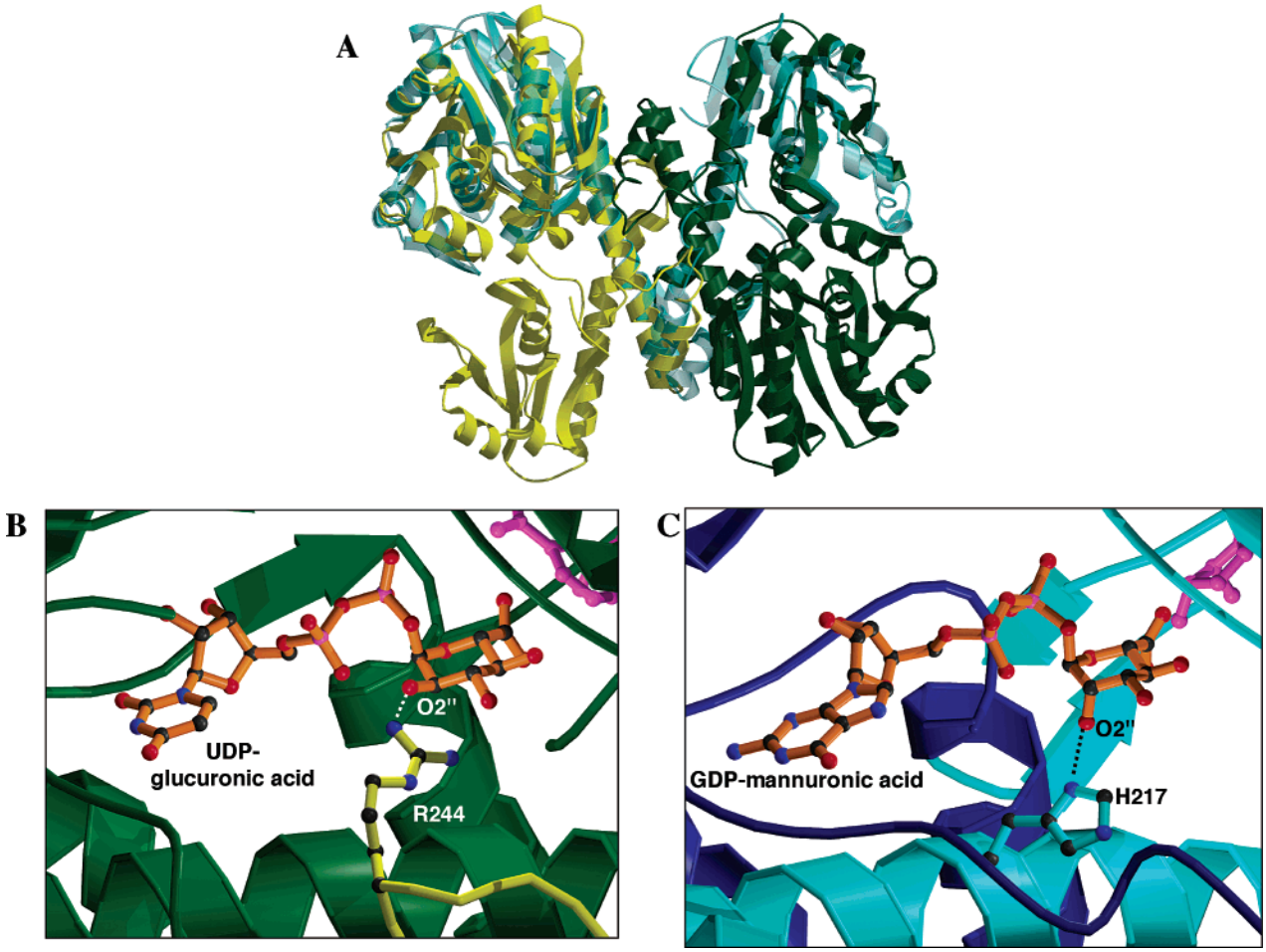

FIGURE 4: Comparison of the structures and sugar nucleotide binding sites of *P. aeruginosa* GMD and *S. pyogenes* UGD. (A) The dimer of UGD, with monomer A in yellow and monomer B in green. Monomer A of GMD is superimposed and shown in semi-transparent cyan. (B) UDP-glucuronic acid in the UGD active site, with the glucose-specific contact made by $Arg244_U$. Colors as in panel A. (C) GDP-mannuronic acid with the mannose-specific contact by His217. Monomer A is shown in cyan, monomer B in blue.

specific binding pocket since all potential hydrogen bonds with the guanine-specific functional groups at positions 2 and 6 of the base are fulfilled. Many of the contacts are made by backbone atoms of the protein, which would tend to limit the accommodation of different orientations and types of bases. GMD is known to discriminate between substrates containing guanine and those with other bases (*12*).

Residues outside the 3-helix cluster of GMD's C-terminal domain also contribute to binding of GDP-mannuronic acid. Four residues in the connecting α-helix of monomer A (Lys210, Asn214, His217, and Asn225) contact the mannuronic acid moiety. Surprisingly, although the C-terminal domain contains a nearly complete dinucleotide-binding fold, only one residue (Lys324) from this region makes a direct hydrogen bond to the GDP-mannuronic acid. This residue is found in an extended loop (residues 320−333), which is structurally equivalent to the phosphate-binding loop of the N-terminal domain. The side chain of Lys324 contacts the pyrophosphate of GDP-mannuronic acid, and so despite the different lengths and sequences, the general structural role of the loop is conserved between the two domains. A single residue from the N-terminal dinucleotide-binding fold, Glu161, contacts the product directly, hydrogen bonding with the pyrophosphate through its main chain amide. The orientation of this residue appears to be stabilized by unusual backbone angles in Ser162 that brings its side chain hydroxyl within 2.6 Å of the main chain carbonyl of Glu161, forming a tight turn. Ser162 is the only nonglycine residue whose ΦΨ angles lie in the generously allowed region of the Ramachandran plot for all four chains in the asymmetric unit. Several other residues in the N-terminal domain of GMD (Thr124, Leu159) make water-mediated contacts to GDP-mannuronic acid.

In addition to the residues important for specific binding of the individual ligands, a complex network of direct and water-mediated hydrogen bonds links NAD(H) and GDP-mannuronic acid within their large binding pocket (Figure 3C). The closest approach of the two ligands is between the nicotinamide ring of NAD(H) and the mannuronic acid moiety of GDP-mannuronic acid, as required for catalysis. Only one residue, Glu161, appears to contact both the cofactor and the product directly, acting as a hydrogen bond donor to GDP-mannuronic acid and as a hydrogen bond acceptor in the modeled interaction with the nicotinamide ring of NAD(H). Glu161 makes an additional water-mediated contact to NAD(H). Another multi-ligand interaction is made by a water molecule tetrahedrally coordinated by Thr124 of monomer A, Asp272 of monomer B, the NO2′ hydroxyl of NAD(H), and O6A″ of the GDP-mannuronic acid carboxylate. This ligand-spanning network of hydrogen bonds in the active site is most likely critical for precise positioning of the cofactor and product during the multistep reaction and

Table 3: Enzyme−Ligand Hydrogen Bond Contacts[a]

chain	domain	protein residue/atom	NAD(H) atom	distance (Å)
A	N-ter	Tyr 10 N	AO2	3.3
A	N-ter	Val 11 N	NO2	3.0
A	N-ter	Asp 30 OD1	AO2′	2.5
A	N-ter	Asp 30 OD2	AO3′	2.7
A	N-ter	Lys 35 NZ	AO3′	2.7
A	N-ter	Val 84 O	NO3′	3.3
A	N-ter	Thr 86 OG1	NO3′	2.7
A	N-ter	Thr 124 N	NO3′	3.1
A§	N-ter	Glu 161 OE1	NN7	
B	C-ter	Lys 271 NZ	NO2′	2.8
B	C-ter	Arg 331 NH1	NO1	3.1
B	C-ter	Arg 331 NH2	NO1	2.9
		water-mediated		
A	N-ter	Gly 9 N	NO2	3.0, 2.8
A	N-ter	Gly 12 N		3.0, 2.8
A	N-ter	Cys 83 O		2.7, 2.8
A	N-ter	Lys 35 NZ	AO2	2.8, 2.5
A	N-ter	Glu 105 OE1	AN1	2.5, 2.7
A‡	N-ter	Thr 124 OG1	NO2′	2.8, 2.7
B‡	C-ter	Asp 272 OD2		2.6, 2.7
A	N-ter	Glu 161 OE2	NO1	2.7, 2.7
B	C-ter	Ser 267 O	NO1	3.0, 2.9

chain	domain	protein residue/atom	GMA atom	distance (Å)
A	N-ter	Glu 161 N	O2B	3.0
A	con. helix	Lys 210 NZ	O6A″	2.9
A	con. helix	Asn 214 ND2	O6A″	2.9
A	con. helix	His 217 ND1	O2″	2.9
A	con. helix	Asn 225 OD1	N2	3.2
B	C-ter	Tyr 256 OH	O2A	2.7
B	C-ter	Tyr 257 OH	O1A	2.6
B	C-ter	Arg 259 N	O6	3.0
B	C-ter	Arg 259 O	N2	3.3
B	C-ter	Phe 262 O	N2	3.0
B	C-ter	Gly 265 N	O3′	2.9
B	C-ter	Lys 324 NZ	AO2	2.8
		water-mediated		
A‡	N-ter	Thr 124 OG1	O6A″	2.8, 3.0
B‡	C-ter	Asp 272 OD2		2.6, 3.0
A	N-ter	Leu 159 O	O6B″	2.9, 3.2
A	N-ter	Glu 161 N	O2B	3.2, 2.6
B	C-ter	Ser 267 OG		3.4, 2.6
B	C-ter	Tyr 257 N	O6A″	3.0, 2.7
			N7	3.0, 3.0
B	C-ter	Phe 262 O	N3, O2′	3.3, 2.8
B	C-ter	Ala 263 O		2.9, 2.8
B	C-ter	Gly 265 O		2.9, 2.7
B	C-ter	Cys 268 N	O3B	3.0, 2.7
B	C-ter	Leu 269 N		2.8, 2.7
B	C-ter	Phe 323 O	O2′	2.8, 3.0
			O3′	2.8, 2.8

[a] Contacts are listed sequentially by protein residue, except for water-mediated contacts where residues contacting the same water are grouped together and indicated with brackets. Distances for the active site formed by the N-terminal domain of chain A and C-terminal domain of chain B are listed; similar values are found in the other three active sites in the asu. The two numbers listed for water-mediated contacts indicate the protein-to-water and water-to-ligand distances, respectively. GMA = GDP − mannuronic acid. ‡Indicates water molecule shared between the two ligands. §Indicates modeled interaction with nicotinamide ring.

may also play a role in communication between the two halves of the active site and the two monomers in the GMD dimer.

Comparison with UDP-Glucose Dehydrogenase. GMD shares mechanistic and sequence similarity with the enzyme UDP-glucose dehydrogenase. The UGD family of enzymes is widespread, found in organisms from bacteria to humans, and functions in a variety of biosynthetic pathways. The structure of one member of this family is known (*10*), that of UGD from *S. pyogenes*, which is involved in synthesis of the anti-phagocytic capsule of this Gram-positive bacterium (PDB codes 1DLI and 1DLJ). A comparison of the sequences of *P. aeruginosa* GMD with *S. pyogenes* UGD (402 amino acids) shows limited but significant sequence similarity extending over nearly the entire protein (22% identity over 395 residues). The conserved N-terminal dinucleotide-binding motif is detectable in both sequences, as are key active site residues in the C-terminal domain (*36*). Although GMD has an extension of 34 residues at its C-terminus relative to UGD, there are no gaps longer than 10 amino acids in the alignment. A superimposition of the two structures shows that the N- and C-terminal domains of both enzymes are quite similar with an rmsd of 1.2 Å^2 for 156 C_α pairs and 1.6 Å^2 for 113 C_α pairs, respectively (Figure 4A). Minor differences in topology between GMD and UGD occur in the dinucleotide-binding fold of the C-terminal domain: GMD is missing strand 3 and helix 5 of the motif, whereas UGD lacks strand 6 and helix 5. In the following paragraphs, we distinguish residues in UGD from those in GMD, by following the residue names with a U (e.g., $Met1_U$).

The major difference in structure between the two enzymes is the dramatic change in domain packing that results in the domain-swapped dimer of GMD. Despite this, the overall arrangement of the GMD dimer is also quite similar to the nonswapped UGD dimer (Figure 4A, rmsd = 1.8 Å^2 for 559 C_α pairs in the dimer). Several small changes combine to allow this rearrangement within an otherwise similar structural context. Relative to the structure of UGD, the domain swap of GMD can be accomplished by changing the backbone angles of several residues in the C-terminal domain. These fall in a 6-residue loop between Asp248 and Leu253 (between helices 1 and 2 of the 3-helix cluster). In accordance with other domain-swapped structures, we call this region the hinge loop. Except for residues 249 and 250, the sequence of the hinge loop is identical in the three known GMD sequences. Asp248 appears to play a particularly important role with both main chain and side chain atoms making hydrogen bonds that determine the conformation of the loop. In UGD, the region corresponding to the hinge loop of GMD is a highly conserved turn that is two residues shorter in length. This turn contains $Arg244_U$: the single residue from monomer A of UGD that contacts the active site of monomer B. This residue has been proposed to be a determinant of substrate specificity since the known GMD proteins have a lysine at the analogous position (*10*). However, because of the domain swapping, Lys250 is not in position to contact the substrate, and no cross-dimer contact analogous to that made by $Arg244_U$ occurs. The extra two residues in GMD's hinge loop may allow the polypeptide chain to form a more flexible loop, rather than the tight turn found in UGD, and could perhaps facilitate formation of the open monomer to allow dimerization.

A survey of domain-swapped structures (*37*, *38*) shows that it is unusual to find a swapped and nonswapped pair with the same oligomeric state, such as the dimers of GMD and UGD. In this circumstance, it is more difficult to rationalize the evolutionary advantage conferred by the domain-swapping event. Indeed, the structure of the UGD

dimer shows a mechanism for intersubunit communication, primarily mediated by $Arg244_U$, which is consistent with the modest cooperative behavior of the enzyme (*10*). In the case of GMD, however, the domain swapping generates a genuinely hybrid active site, with residues from both polypeptide chains contributing about equally to surface area and hydrogen bonding to ligands. This greatly enhances opportunities for intersubunit communication and is potentially related to the complicated cooperativity exhibited by the enzyme (*11*). Another potential effect of the domain swapping is increased stability of the dimer. The dimer interface of UGD is primarily mediated by contacts between the connecting α-helices and is quite substantial: more than 2600 Å^2 of surface area (*10*). However, the contact area between the two chains of the GMD dimer is more than twice that of UGD: 5950 Å^2, accounting for nearly 30% of the total surface area of the monomer. Confirmation of increased dimer stability awaits experimental determination of the association constants of the two proteins.

The availability of two high-resolution structures for GMD and UGD, both in ternary complex with cofactor and product, allows for the first time a detailed comparison of the active sites of these two enzymes. Consistent with their overall structural similarity, GMD and UGD share generally similar modes of ligand binding. This can be demonstrated by a superposition of the backbone atoms of the two dimers that results in nearly identical orientation of cofactor and product in the binding pocket (data not shown). While many protein−ligand contacts are conserved, analysis of the substrate binding sites reveals striking differences that account for the differences in sugar specificities in these two enzyme families (Figure 4B,C). Because glucose and mannose are epimers at C2″, contacts with the O2″ hydroxyl group are potentially critical for substrate recognition. In the UGD complex, O2″ of the glucuronic acid points up toward the opening of the active site and is contacted by $Arg244_U$ from the opposite dimer pair. As mentioned above, the equivalent residue in GMD, Lys250, cannot make a similar contact because of domain swapping. Furthermore, in the GMD complex, the O2″ of mannuronic acid points down into floor of the active site, where it makes a hydrogen bond with the side chain of His217. The orientation of this histidine ring is anchored by a second hydrogen bond with the side chain of Asn252, a conserved residue in the hinge loop. In the UGD structure, a hydrophobic residue ($Leu211_U$) is found at the position equivalent to His217, which makes van der Waals contacts with the ring carbon C2″. This arrangement would be predicted to exclude mannose-based substrates from the UDP-glucose binding pocket, although to the best of our knowledge this has not been tested experimentally. For GMD, the opposite is not true since there appears to be room for glucose-based molecules to bind in the pocket, although the hydrogen bond to His217 would be unfulfilled. In fact, GDP-glucose has been reported to be an inhibitor of GMD but not a substrate (*12*). Site-directed mutagenesis can be used to confirm the apparent striking correlation between the structures and the binding specificities of these two enzymes.

Implications for Enzyme Mechanism. The reaction catalyzed by GMD is a 4-electron oxidation proposed to proceed via the pathway shown in Figure 1A (*12*). Two equivalents of NAD^+ are utilized to convert substrate to product in a bi uni uni bi ping-pong reaction mechanism. The reaction has four discrete steps: (1) oxidation of the substrate C6″ hydroxyl to an aldehyde; (2) nucleophilic attack by an active site thiol to form a thiohemiacetal intermediate; (3) oxidation of the tetrahedral thiohemiacetal to a thioester; and (4) hydrolysis of the thioester to product. The proposed mechanism requires protein residues to fulfill the roles of active site thiol and general/acid base catalyst. It also necessitates binding and release of NAD^+/NADH without dissociation of the nucleotide sugar intermediates. The crystal structure of GMD provides new insights into this complex, multistep reaction.

On the basis of sequence alignments and comparison with the UGD structure, Cys268 of GMD was proposed to be the nucleophilic thiol (*10*, *12*). The importance of this residue is consistent with the sensitivity of the enzyme to thioreactive reagents and a Cys268 to serine mutation that reduces enzyme activity by 95% (*6*). In the crystal structure, distances between the Cys268 thiol group and the oxygens of the carboxylate group of the mannuronic acid are between 3.3 and 3.5 Å. However, rotation of the cysteine side chain brings Sγ to within 2.4 Å of O6A″. Because it is such a potent nucleophile, it is presumed that the thiolate anion of Cys268 serves as the active species in formation of the putative thiohemiacetal intermediate. Since a typical pK_a for a cysteine side chain is ∼9.0, factors stabilizing the thiolate anion would be expected in the active site. One possibility for this would be a positively charged residue in the vicinity that could perturb the pK_a of the cysteine side chain downward. The basic residue nearest to Cys268 is Lys 271. The Nζ group of this residue hydrogen bonds to NAD(H), Asp272, and Thr86 and is ∼5 Å from the Cys268 thiol. However, rotation of the lysine side chain can bring it within 3.0 Å of Sγ. Another possible stabilizing factor is a helix dipole effect. Cys268 is located immediately prior to an α-helix (residues 269−282) in the C-terminal domain and could thus be influenced by the partial positive charge of the dipole. Activation of a catalytic thiol via the helix dipole effect has been proposed in the case of β-ketoacyl-acyl carrier protein synthase III from *E. coli* (*39*) and shown to lower the pK_a of cysteine side chains in synthetic peptides by nearly two units (*40*). The presence of a negatively charged residue at the N-terminus of a helix can partially neutralize the dipole, but such a residue is not found in GMD; thus, the full effect of the dipole should be present.

Two possible candidates for the general acid/base catalyst expected to assist with hydride transfer are suggested by the crystal structure. One of these is Lys210 from monomer A, whose terminal Nζ atom is 2.9 Å from O6A″ of the mannuronic acid carboxylate. This residue is in position to act as general base by abstracting a proton from the C6″ hydroxyl group of GDP-mannose and also from the thiohemiacetal intermediate. It could presumably also act as a general acid and donate a proton to stabilize the tetrahedral intermediate formed from the aldehyde. Alternatively, a water molecule could play the role of general acid/base. The best candidate for this is the water tetrahedrally coordinated by Asp272, Thr124, a hydroxyl of the nicotinamide ribose, and O6B″ of GDP-mannuronic acid (Figure 3C). Coordination by Asp272 could help activate this water molecule for nucleophilic attack; the position of the Asp272 side chain appears to be anchored by a hydrogen bond with Asn214.

Analogous possibilities for the acid/base catalyst were suggested for UGD dehydrogenase, emphasizing the overall structural similarity of the active sites in these enzymes (*10*). However, in the UGD structure, all of these residues are on the same monomer, while in GMD some of these residues come from monomer A and others from monomer B.

The crystal structure of GMD also suggests a candidate residue for assisting in the final step of the reaction: hydrolysis of the thioester intermediate to GDP-mannuronic acid. It is likely that an ionizable residue in the active site helps activate a water molecule for attack on the thioester. To be properly positioned for attack, this residue should be located on the opposite side of the mannuronic acid carboxylate group, relative to the general acid/base that assists with hydride transfer. The side chain of Glu157 is found in this vicinity, less than 3 Å from one of the carboxylate oxygens of the mannuronic acid moiety. Although it does not interact with a water molecule in the present structure, small structural rearrangements between the enzyme−thioester and enzyme−product complexes could easily allow for this.

A requirement of the two-step oxidation catalyzed by GMD is binding and dissociation of NAD^+/NADH, while the substrate remains in the active site. On the basis of the small patch of solvent-exposed surface on the purine bases, each ligand appears to have its own entrance/exit for binding in the active site of GMD, which is not obscured in either the dimeric or the tetrameric oligomers. This would appear to permit binding and release of NAD(H) without disturbing the nucleotide sugar. However, since both NAD(H) and GDP-mannuronic acid are highly buried in their binding pockets, a significant change in protein conformation seems necessary to permit release of either ligand. In the case of UGD, this has led to postulation of flexible loops or gate regions in the protein and is consistent with apparent difficulty in crystallization of apo-forms of the protein (*10*). The apparent requirement for protein conformational flexibility in ligand binding and release raises an important question: if the cofactor is free to bind and dissociate during the reaction, what prevents dissociation of the aldehyde intermediate from the enzyme? The simplest explanation for this phenomenon is kinetic: if the aldehyde is trapped very rapidly by the thiolate anion to form the covalently linked thiohemiacetal, flux through the competing pathway represented by dissociation of the aldehyde would be negligible. Mechanistic studies to determine the validity of this hypothesis are underway.

Because of its critical role in alginate biosynthesis and biofilm formation, GMD is a logical target for clinical inhibitors to fight *P. aeruginosa* infections. The crystal structure opens new avenues for structure-based inhibitor design of this enzyme. Both the domain swapping and the observed tetrameric arrangement of the enzyme were unexpected and highlight the importance of direct structural information on individual targets. The high-resolution structural information on the active site has revealed residues critical for substrate specificity and will aid in the process of inhibitor design. Several commercially available compounds are known inhibitors of GMD, including penicillic acid and macrolide antibiotics such as erythromycin (*41*), and are excellent initial candidates for complex formation and structural characterization. The GMD structure also serves as a model for other members of this enzyme family, including GMD from the plant pathogen *P. syringae*. Additional GMD proteins are likely to be identified as more bacterial genomes are sequenced. Finally, since the structures and mechanisms of two enzymes in the alginate biosynthetic pathway of *P. aeruginosa* have now been characterized (*42*, *43*), the opportunity for targeting multiple steps in the pathway is available and should lead to a better understanding of the pathogenicity of this organism.

ACKNOWLEDGMENT

We thank Laura Naught, Gina Hoey, and Jennifer Kimmel for assistance with protein purification and Jack Tanner and Todd Yeates for helpful discussions. We acknowledge the staff of the Structural Biology Center at beam line 19-ID of the Advanced Photon Source of Argonne National Laboratory for synchrotron time and technical assistance.

REFERENCES

1. Yu, H., and Head, N. E. (2002) *Front. Biosci. 7*, D442−57.
2. Pier, G. B. (1997) *Behring Inst. Mitt.* 350−60.
3. Hentzer, M., Teitzel, G. M., Balzer, G. J., Heydorn, A., Molin, S., Givskov, M., and Parsek, M. R. (2001) *J. Bacteriol. 183*, 5395−401.
4. Tatnell, P. J., Russell, N. J., and Gacesa, P. (1993) *J. Gen. Microbiol. 139*, 119−27.
5. Elloumi, N., Moreau, B., Aguiar, L., Jaziri, N., Sauvage, M., Hulen, C., and Capmau, M. L. (1992) *Eur. J. Med. Chem. 27*, 249−54.
6. Shankar, S., Ye, R. W., Schlictman, D., and Chakrabarty, A. M. (1995) *Adv. Enzymol. RAMB. 70*, 221−55.
7. Tavares, I. M., Leitao, J. H., Fialho, A. M., and Sa-Correia, I. (1999) *Res. Microbiol. 150*, 105−16.
8. Tabernero, L., Bochar, D. A., Rodwell, V. W., and Stauffacher, C. V. (1999) *Proc. Natl. Acad. Sci. U.S.A. 96*, 7167−71.
9. Barbosa, J. A., Sivaraman, J., Li, Y., Larocque, R., Matte, A., Schrag, J. D., and Cygler, M. (2002) *Proc. Natl. Acad. Sci. U.S.A. 99*, 1859−64.
10. Campbell, R. E., Mosimann, S. C., van De Rijn, I., Tanner, M. E., and Strynadka, N. C. (2000) *Biochemistry 39*, 7012−23.
11. Naught, L. E., Gilbert, S., Imhoff, R., Snook, C., Beamer, L., and Tipton, P. (2002) *Biochemistry 41*, 9637−45.
12. Roychoudhury, S., May, T. B., Gill, J. F., Singh, S. K., Feingold, D. S., and Chakrabarty, A. M. (1989) *J. Biol. Chem. 264*, 9380−5.
13. Van Duyne, G. D., Standaert, R. F., Karplus, P. A., Schreiber, S. L., and Clardy, J. (1993) *J. Mol. Biol. 229*, 105−24.
14. Otwinowski, Z., and Minor, W. (1997) *Methods Enzymol. 276*, 307−26.
15. Terwilliger, T. C., and Berendzen, J. (1999) *Acta Crystallogr. D 55*, 849−61.
16. Terwilliger, T. C. (2000) *Acta Crystallogr. D 56*, 965−72.
17. Jones, T. A., Zou, J. Y., Cowan, S. W., and Kjeldgaard, M. (1991) *Acta Crystallogr. A 47*, 110−9.
18. Murshudov, G. N., Vagin, A. A., Lebedev, A., Wilson, K. S., and Dodson, E. J. (1999) *Acta Crystallogr. D 55*, 247−55.
19. Winn, M. D., Isupov, M. N., and Murshudov, G. N. (2001) *Acta Crystallogr. D 57*, 122−33.
20. No. 4, C. C. P. (1994) *Acta Crystallogr. D 50*, 760.
21. Kissinger, C. R., Gehlhaar, D. K., and Fogel, D. B. (1999) *Acta Crystallogr. D 55*, 484−91.
22. Laskowski, R. A., McArthur, M. W., Moss, D. S., and Thornton, J. M. (1993) *J. Appl. Crystallogr. 26*, 283−91.
23. Hooft, R. W., Vriend, G., Sander, C., and Abola, E. E. (1996) *Nature 381*, 272.
24. Vaguine, A. A., Richelle, J., and Wodak, S. J. (1999) *Acta Crystallogr. D 55*, 191−205.
25. Colovos, C., and Yeates, T. O. (1993) *Protein Sci. 2*, 1511−9.
26. Liang, J., Edelsbrunner, H., and Woodward, C. (1998) *Protein Sci. 7*, 1884−97.
27. Jones, S., and Thornton, J. M. (1996) *Proc. Natl. Acad. Sci. U.S.A. 93*, 13−20.
28. Lu, G. (2000) *J. Appl. Crystallogr. 33*, 176−83.
29. Kraulis, P. (1991) *J. Appl. Crystallogr. 24*, 946−50.

30. Altschul, S. F., Gish, W., Miller, W., Myers, E. W., and Lipman, D. J. (1990) *J. Mol. Biol. 215*, 403−10.
31. Kutzenko, A. S., Lamzin, V. S., and Popov, V. O. (1998) *FEBS Lett. 423*, 105−9.
32. Bennett, M. J., Schlunegger, M. P., and Eisenberg, D. (1995) *Protein Sci. 4*, 2455−68.
33. Roychoudhury, S., Chakrabarty, K., Ho, Y. K., and Chakrabarty, A. M. (1992) *J. Biol. Chem. 267*, 990−6.
34. Bottoms, C. A., Smith, P. E., and Tanner, J. J. (2002) *Protein Sci. 11*, 2125−37.
35. Bellamacina, C. R. (1996) *FASEB J. 10*, 1257−69.
36. Dougherty, B. A., and van de Rijn, I. (1993) *J. Biol. Chem. 268*, 7118−24.
37. Newcomer, M. E. (2002) *Curr. Opin. Struct. Biol. 12*, 48−53.
38. Schlunegger, M. P., Bennett, M. J., and Eisenberg, D. (1997) *Adv. Protein Chem. 50*, 61−122.
39. Davies, C., Heath, R. J., White, S. W., and Rock, C. O. (2000) *Structure Fold. Des. 8*, 185−95.
40. Kortemme, T., and Creighton, T. E. (1995) *J. Mol. Biol. 253*, 799−812.
41. Nakagawa, A., Hosoyama, T., Chubachi, K., Takahashi, S., Ohkubo, T., and Iyobe, S. (1997) *J. Antibiot. (Tokyo) 50*, 286−8.
42. Naught, L. E., and Tipton, P. A. (2001) *Arch. Biochem. Biophys. 396*, 111−8.
43. Regni, C., Tipton, P. A., and Beamer, L. J. (2002) *Structure Fold. Des. 10*, 269−79.

BI027328K